A R C H I V E S O F M E T A L L U R G Y A N D M A T E R I A L S
Volume 60 2015 Issue 1
DOI: 10.1515/amm-2015-0021

H. PAUL*, A. MORAWIEC*, T. BAUDIN**, T. CZEPPE*

TEM STUDY OF RECRYSTALLIZATION IN ULTRA-FINE GRAIN AA3104 ALLOY PROCESSED BY HIGH-PRESSURE TORSION

ANALIZA PROCESU REKRYSTALIZACJI W STOPIE AA3104 PRZETWARZANYM W PROCESIE HPT Z WYKORZYSTANIEM TECHNIK TRANSMISYJNEJ MIKROSKOPII ELEKTRONOWEJ

The effect of annealing on the microstructure and the texture development was investigated in a particle containing AA3104 aluminium alloy. The samples were processed at room temperature by high-pressure torsion (HPT) up to ten turns. The nucleation of new grains was analyzed by a transmission electron microscope equipped with a system for local orientation measurements and a heating holder.

The shear deformation induces a decrease of the grain size. After the first two turns of the HPT processing the initial structure of large grains was 'transformed' into a structure of fine cells/grains with the diameter of a few tens of nanometers. In the central areas of the samples the elongated shape of the cells/grains was observed up to six turns. For higher deformations, this structural inhomogeneity was totally removed and only the equiaxed grains were observed. The crystal lattice of small grains rotates in such a way that the <111> direction is parallel to the compression axis. After annealing the structure coarsened. Nevertheless, after primary recrystallization, the structure was still composed of relatively fine and equiaxed grains of a similar size. In most of the observed cases the size of the recrystallized grains in the areas close to and far from the large second phase particles was similar. The recrystallization leads to the creation of new texture components. The new grain orientations lost the positions typically observed in the deformed state and showed the tendency for the coincidence of the <100> crystallographic directions with the compression axis.

Keywords: High Pressure Torsion, AA3104 alloy, TEM orientation mapping, Texture, Microstructure

W pracy analizowano wpływ warunków wyżarzania na zmiany mikrostrukturalne i teksturowe w stopie AA3104 zawierającym wydzielenia cząstek drugiej fazy. Próbki odkształcano z wykorzystaniem techniki skręcania pod wysokim ciśnieniem (HPT), do dziesięciu obrotów, w temperaturze otoczenia. Proces zarodkowania nowych ziaren analizowano z wykorzystaniem transmisyjnej mikroskopii elektronowej wyposażonej w system pomiaru orientacji lokalnych oraz *'heating holder'*.

Zaobserwowano, że w miarę wzrostu liczby obrotów, intensywne ścinanie prowadzi do silnego zmniejszenia wielkości ziarna. Po dwu obrotach, wyjściowa struktura dużych ziaren uległa przekształceniu w strukturę drobnoziarnistą złożoną z ziaren o wielkości kilkudziesięciu nanometrów. W obszarach próbki zbliżonych do osi obrotu wydłużony kształt ziaren obserwowano do sześciu obrotów. W zakresie wyższych stopni odkształcenia ta niejednorodność strukturalna zanika; obserwowano jedynie równoosiowe ziarna. Orientacja sieci krystalicznej tych ziaren formuje silną teksturę osiową z kierunkiem <111> usytuowanym równolegle do kierunku normalnego (osi ściskania/skręcania). Po wyżarzaniu struktura ulega 'pogrubieniu'. Jednakże, w zakresie rekrystalizacji pierwotnej, w dalszym ciągu pozostaje równoosiowa i silnie rozdrobniona. W większości obserwowanych przypadków wielkość zrekrystalizowanych ziaren w obszarach położonych zarówno w pobliżu, jak i w znacznej odległości od dużych wydzieleń cząstek drugiej fazy, była na zbliżonym poziomie. Proces wyżarzania prowadzi do pojawienia się nowych składowych tekstury. Orientacje nowych ziaren są odmienne od tych, jakie obserwowano w stanie zdeformowanym i wykazują silną tendencję do sytuowania kierunku <100> równolegle do osi ściskania/skręcania.

1. Introduction

Severe plastic deformation (SPD) has been widely used for the conversion of conventional coarse-grained bulk materials into ultra-fine grained polycrystals [1-3]. Various discontinuous and continuous SPD techniques available for grain refinement are described in the literature, and significant interest has been focused on equal channel angular pressing (ECAP), high pressure torsion (HPT), accumulative roll-bonding, multiple forging or their combinations. However, only HPT processing presents the opportunity for achieving an exceptional grain refinement, often up to the scale of tens of nanometers. The main disadvantage against a wider use of this method is that the manufactured samples are rather small and usually in the form of relatively thin discs. It is so despite various modifications of the deformation set-up have been proposed for the purpose of enlarging the manufactured samples, e.g. [2].

* POLISH ACADEMY OF SCIENCES, INSTITUTE OF METALLURGY AND MATERIALS SCIENCE, 30-059 KRAKOW, 25 REYMONTA ST., POLAND
** UNIVERSITÉ PARIS-SUD, ICMMO, CNRS UMR 8182, LABORATOIRE DE PHYSICO-CHIMIE DE L'ETAT SOLIDE, ORSAY, F-91405, FRANCE

HPT is a continuous process and its principles are illustrated schematically in Fig. 1a. The sample in the form of a thin disc is located between two anvils and then subjected to compressive pressure of several GPa (usually at room temperature). Simultaneously, the sample is subjected to torsional strains which are imposed through a rotation of the lower anvil. Therefore, surface frictional forces deform the disc by shear so the deformation proceeds under quasi-hydrostatic pressure.

The literature data concerning the mechanical properties of the HPT-processed Al and its alloys is relatively rich, e.g. [4-17]. Earlier investigations, thoroughly summarized in [2], showed that the strength properties increase as the number of turns and/or the pressure increases. The strong increase of the dislocation density, and hence the stored energy of the plastic deformation, are crucial for the above changes. It is well-documented that the (micro)hardness increases and the grain size decreases drastically just after one turn. It was also noticed that the hardness and the grain diameter reach the saturation values very quickly, as presented many times in the past, e.g. [2]. When investigating the structure of the samples subjected to HPT, it is important to note that the central region of the disk is not refined to the same extent as the outer region. The inhomogeneity associated with the grain refinement and the decrease of strength in the central region is gradually removed as the number of turns increases; the values of microhardness and the average grain sizes in the central and outer regions are relatively similar just after a total of 5-6 turns [2]. The intensity of the structure refinement and the sample strengthening also strongly depend on the applied deformation route, as showed recently by Zhang et al [6] for different aluminium alloys.

From the practical point of view, it is important that the microstructures obtained via HPT remain reasonably refined and homogeneous after heating to the temperature of further plastic shaping. In particle containing aluminium alloys, the non-uniform distribution of strains, resulting from the formation of highly deformed zones around large particles, leads to a non-homogeneous distribution of the grain sizes after further annealing, e.g. [18, 19]. This morphological differentiation coincides with drastic textural changes [20]. The issue of a new orientation 'generated' during annealing of deformed metals of 'conventional grain size' has been investigated extensively for several years. There are only a few works, e.g. [21-23] which discuss the crystallographic aspect of recrystallization nucleation in extremely fine-grained materials.

The present study is focused on the analysis of the microstructure evolution and the texture transformations that occur during the HPT-processing and further annealing of the AA3104 alloy. The novelty of the present work is that both aspects of the new grain occurrence were investigated by a system of local orientation measurements in transmission electron microscopy (TEM) combined with TEM *in-situ* heating. TEM provides the opportunity of continuous observation of the changes occurring during annealing. It is crucial for the correct interpretation of the microstructure and texture transformations.

2. Experimental procedures

The material used in the investigations was a particle containing AA3104 (Al-1.27Mg 1.05Mn 0.43Fe 0.23Ti 0.20Si 0.15Cu) aluminium alloy. The cast ingot was homogenized and then hot rolled on an industrial reversing mill to a 20 mm thickness plate.

Samples of 13 mm in diameter and 1.8 mm in height were cut-off from the initial material. The samples were deformed *via* HPT up to ten turns at room temperature under the pressure of 2 GPa and 3 GPa. The rotational speed was about one turn per minute, thereby any heat generated in the sample was quickly conducted away. In each case, the compression plane of the HPT processing in the Bridgman anvil-type unit was parallel to the rolling plane of the initial material.

The morphological changes and the texture transformations occurring during recovery and recrystallization were investigated in two kinds of experiments. Firstly, the samples were annealed in TEM during the *in-situ* recrystallization experiments; the thin foils were recrystallized at the temperature which can be estimated to be about 300°C, for the times ranging between 30 s and 120 s. Secondly, the deformed bulk samples were annealed at 300°C for the times ranging between 30 s and 300 s and then analysed by means of a high resolution scanning electron microscope (SEM) equipped with an electron backscattered diffraction (EBSD) facility.

Following the HPT processing and further annealing, the microstructure observations were undertaken at selected positions of the discs, in the sections perpendicular to the compression plane. In the case of the axial section, the sample section edges were parallel to the normal/axial (ND) and the radial (RD) directions. The thin foils were cut out from the central and the peripheral regions, as shown schematically in Fig. 1b. The 'dimensions of the TEM samples' were 1.8 mm – width (||ND) and 3 mm – length (||RD). An additional analysis was made in the ND-TD section, where TD is the tangential (shear) direction (Fig. 1b). The twin-jet electro-polishing in a standard nitric acid (33%) and methanol (67%) solution, with the use of TenuPol-5, was the last step of the thin foil preparation.

The microstructure observations after the deformation and further annealing were carried out by means of bright field imaging in TEM with the use of a CM20 PHILIPS operating at the nominal voltage of 200 kV. The microscope was equipped with an in-house Kikuchi line-based system for local orientation measurements. The orientation maps were created by the scanning of the interesting area with the step size ranging between 10 nm and 20 nm (and the beam size of 5 nm or 10 nm). In all the cases, the areas of nearly the same foil thickness (~200 nm) were analyzed. The post-processing analysis of the orientation maps was performed with the use of the HKL Technology^{TM} Channel 5 software.

The measurements of the chemical composition changes were performed by means of TEM with the use of an FEI Technai G^2 microscope, operating at the accelerating voltage of 200 kV. The TEM was equipped with a field emission gun and a high-angle annular dark field scanning/transmission detector (HAADF/STEM), combined with an EDAX^{TM} energy dispersive X-ray (EDX) microanalyser.

The collection of orientations over the larger areas was made in a complementary study by SEM with the use of Zeiss Supra 55VP, equipped with a high-resolution EBSD facility. In that case, the microscope control, the pattern acquisition and the indexing were carried out with the TSL OIM^{TM} Analysis 5 software. The SEM local orientation measurements were performed in the sections perpendicular to the compression plane, with the use of the step size of 100 nm. In all the {111} pole figures corresponding to the TEM and SEM orientation maps, the indices {*hkl*}<*uvw*> represent the texture component which has the {*hkl*} plane parallel to the ND-RD or ND-TD plane and the <*uvw*> direction parallel to the ND. The sample co-ordinate system for the HPT-processing and the sample sectioning are presented in Fig. 1.

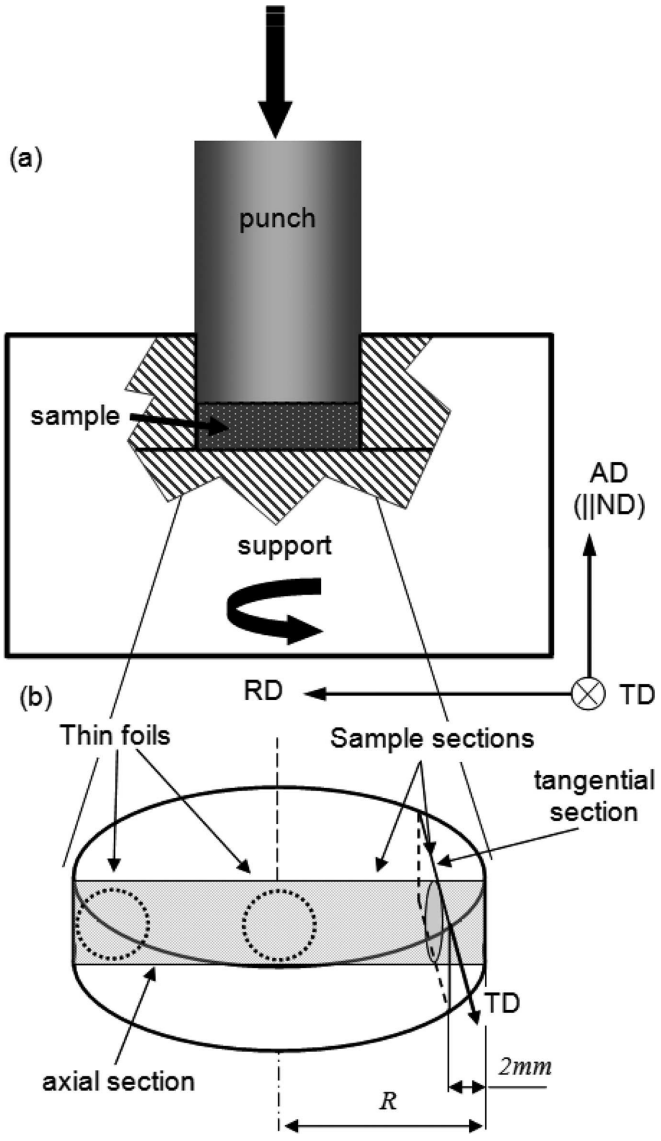

Fig. 1. Schematic presentation of (a) HPT processing and (b) sample sectioning

Measurements by differential scanning calorimetry (DSC) were performed with the heating rate of 10 K/min by means of a TA Instruments Q1000 calorimeter. After holding the sample at 550°C for about 15 min, a second DSC run was performed. This provided the reference baseline for the data analysis.

3. Results

3.1. Microstructure of the initial stage

Figure 2 shows the initial microstructures of the aluminium AA3104 alloy observed in the sections perpendicular to the rolling plane. The initial state of the alloy was characterized by a bimodal distribution of second phase particles (SPPs), i.e. coarse plate-like intermetallics (large SPPs) occurring against the background of fine, mostly globular dispersoids (Figs. 2a and b). Both types of SPPs play an important role in the recrystallization process. Large SPPs are well-known to form highly deformed zones around them, and therefore the surroundings of the large particles are the preferential places for the recrystallization nucleation. Small particles play an important role in the pinning of the recrystallization front. The matrix volumes (solid solution) showed increased contents of Mg, Mn and Cu, whereas both types of particles (large and small SPPs) revealed a significantly more complex chemical composition, due to the significantly higher contents of Mn, Fe, Si with a small addition (in some cases) of Cu and Mg. The energy dispersive X-ray microanalysis in SEM and TEM showed that the plate-like intermetallics were mostly of the AlFeMnSi or Al_6Mn type, whereas the dispersoids were of

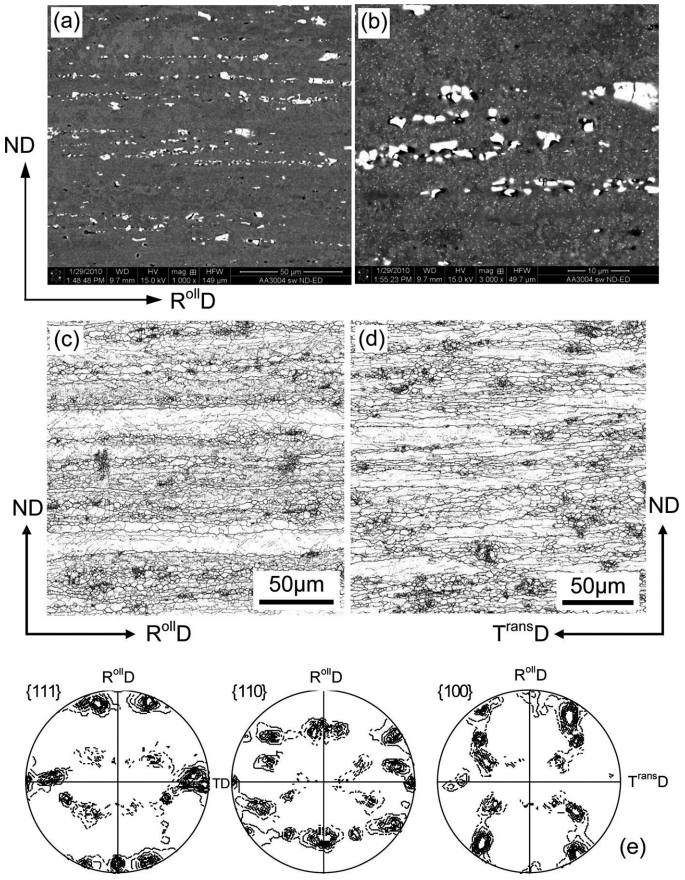

Fig. 2. Initial microstructure of the AA3104 alloy before HPT processing. (a) Layers of large SPPs and (b) randomly distributed dispersoids. SEM imaging in secondary electrons. Grain boundary orientation maps (the boundaries with disorientation angle >1.5^o and >15° are marked) showing microstructure of flat grains observed in: (c) ND-R^{oll}D and (d) ND-T^{rans}D sections and corresponding (e) texture presented in rolling plane. SEM/EBSD local orientation measurements with step size of 100 nm

the AlMnSi, AlMnCu or $CuAl_2$ type, as previously observed in [24-29]. The diameter of the large SPPs had the sizes in the range between 2 μm and 15 μm, whereas those of the fine dispersoids – between 50 nm and 100 nm.

After hot rolling, the material showed a partly recrystallized structure, composed mostly of large flattened grains, as visible in Figs. 2c and d. In both sections perpendicular to the rolling (compression) plane, i.e. ND-R^{oll}D and ND-T^{rans}D, the high angle grain boundaries were situated along R^{oll}D and T^{rans}D, respectively. The ND, R^{oll}D and T^{rans}D describe the normal, rolling and transverse, direction, respectively. The average grain length and thickness were about 100 μm and 20 μm, respectively. At this initial stage the material shows a typical copper type rolling texture, as presented in Fig. 2e.

3.2. Deformation microstructure evolution during HPT processing

Bright field imaging in TEM was applied to reveal the inherent characteristics during the HPT processing. The deformed microstructure was analysed in near peripheral and central regions of the sample. Particular attention was paid to the microstructure evolution due to the increased deformation, to the applied pressure and to the differentiation of the microstructure evolution in the central and peripheral areas. In each case, the microstructure evolution close to and far from the large SPPs was at the heart of the interest.

3.2.1. Areas far from large particles

Figures 3a-c are the TEM bright field micrographs showing the microstructures in the ND-RD section at the periphery of the samples after 2, 6 and 10 turns, under the pressure of 2 GPa. After 2 turns the structure was still inhomogeneous and mostly composed of thin elongated grains/cells[1)] (Fig. 3a). The width of the grains/cell ranged between 150 nm and 200 nm, whereas the length – between 500 nm and 800 nm. The longer axis was situated nearly parallel to the radial direction. After six turns (Fig. 3b) the distribution of the cell/grain sizes becomes fairly uniform and the grains are mostly equiaxed. Starting from these deformations, the grain/cell size tends to get stabilized as the deformation increases. The diameter of a large fraction of the equiaxed grains/cells was significantly below 100 nm. After ten turns, the structure over very large areas was perfectly homogeneous (Fig. 3c), i.e. the bright field image shows only equiaxed grains/cells with the diameter ranging between 50 nm and 100 nm.

The selected area diffraction (SAD) patterns show a difference in the scattering tendency of the orientations of the deformed grains as the deformation increases. After 2 turns, the orientations of the prevailing fraction of the grains can be easily identified. After 6 and 10 turns, the SAD patterns come in concentric rings; this indicates that the aperture selects many small grains with different crystallographic orientations. The comparison of the SAD patterns after 6 and 10 turns also demonstrates peak broadening after the higher deformation, due to the refinement of the grain size and the presence of internal stresses, as observed earlier in [30]. The common feature observed for all the deformation degrees was that the majority of grains was characterized by the <110> crystallographic direction perpendicular to the foil surface.

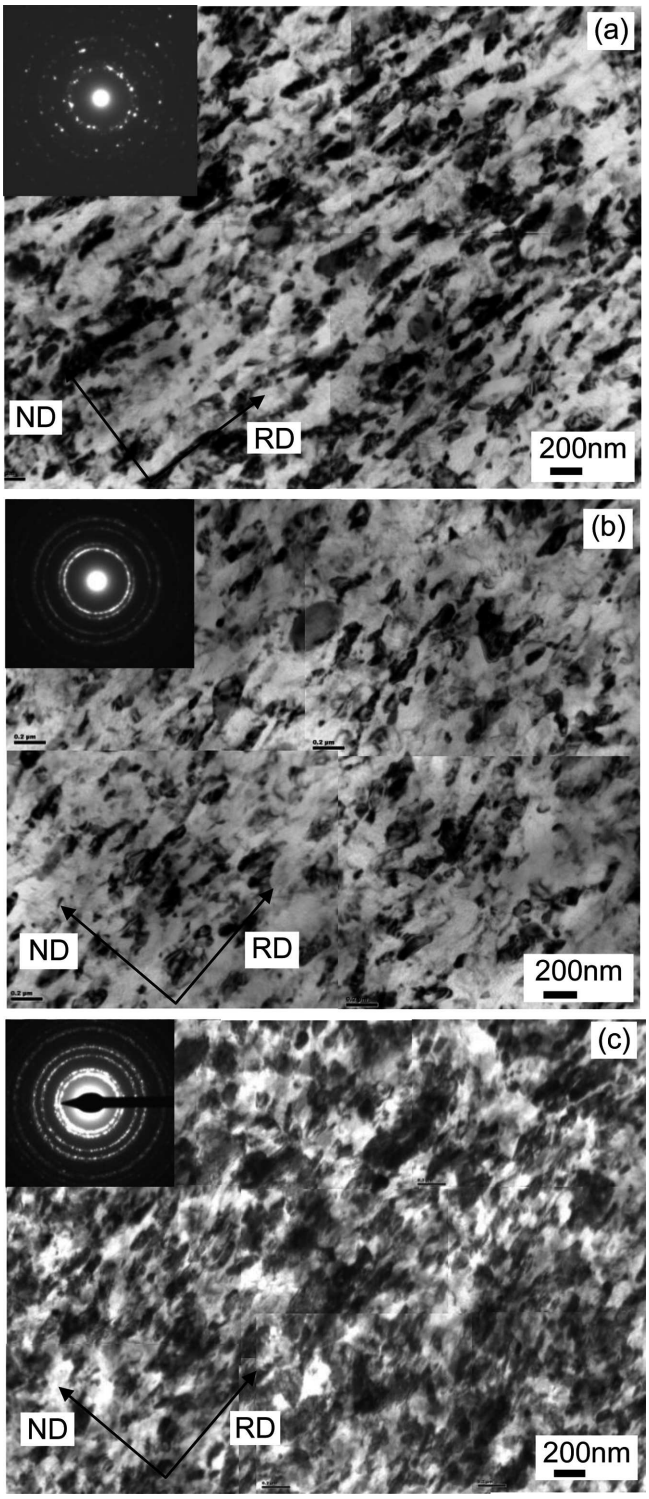

Fig. 3. Microstructure evolution with increasing strain. TEM bright field images observed after: (a) 2, (b) 6 and (c) 10 turns, under 2 GPa pressure. Thin foils cut-out from sample periphery in ND-RD section

The elongated shape of the grains very quickly disappears as the value of pressure increases. Figures 4a-d are the TEM bright field images showing the typical microstructures in the

[1)] it should be noted that the bright field imaging counts all types of boundaries, i.e. low and high angle, without distinction

areas close to the disc centre and to the disc periphery, observed after 4 turns under the pressures of 2 GPa and 3 GPa. It is noticeable that the elongated shape of the grains/cells that dominate in the areas close to the sample centre under the pressure of 2 GPa disappears after the pressure of 3 GPa, for the same number of turns. The processing under the pressure of 3 GPa leads to a microstructure composed of perfectly equiaxed grains of a similar size. (The same trend was often observed in other materials processed by HPT, as shown in, e.g. [2, 31]).

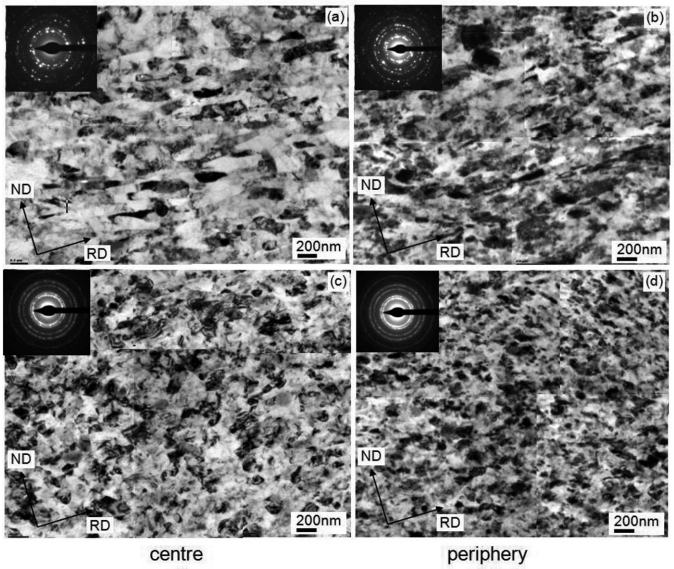

Fig. 4. Microstructures observed after 4 turns under: (a) and (b) 2 GPa pressure, (c) and (d) 3 GPa pressure in (a) and (c) central and (b) and (d) peripheral regions of the sample. TEM bright field imaging in ND-RD section

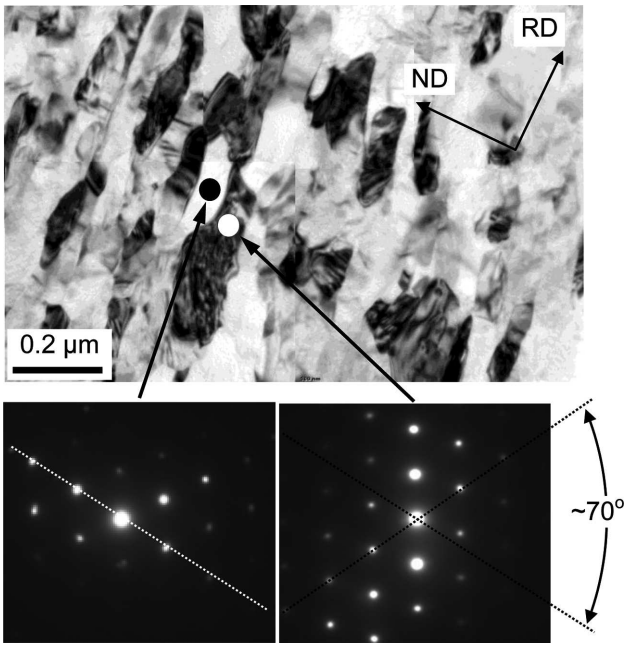

Fig. 5. Microstructure observed in central area of the sample processed in two turns under 2 GPa pressure showing strong disorientations between neighbouring grains. TEM bright field imaging and corresponding SAD patterns

The neighbouring grains were often strongly disoriented. This was revealed by the comparison of the two SAD patterns corresponding to the adjacent grains, both with the beam direction close to the <110> axis (Fig. 5). It is well visible that the orientations of the neighbouring grains were rotated in respect to each other by ~70° around the <110> axis. This clearly indicates that the near-twin relation occurred between those areas (in fact, two complementary oriented grains were detected).

3.2.2. Areas adjacent to large particles

The shear process in the vicinity of the large SPPs led to an extremely strong microstructure refinement. The grains, forming zones 'flowing around' the large particles, were progressively converted into finer ones as the number of turns increased. After ten turns, those small grains had the sizes a few tens of nanometres (usually below 50nm). The zones showed a great tendency for broadening as the number of turns and/or the applied pressure increased (Figs. 6a and b). The structure refinement coincides with the cracking or even fragmentation of the large elongated particles, as observed earlier in the ECAP-processed samples of the same alloy [27, 28].

The width of the zone of the localized strain strongly depends not only on the applied number of turns and the pressure but also on the particle size and shape. It was observed that the smaller particle size, the thinner the zone around them. The detailed bright field image analysis shows that the width of the localized strain zones in most cases varies from ~400 nm after two turns to ~1 μm after 10 turns (at 2 GPa pressure). The strongest disturbances of the matrix occurred inside the volumes where the clustering of large SPPs was observed (Fig. 6c) or at the tips of the large plate-shaped SPPs.

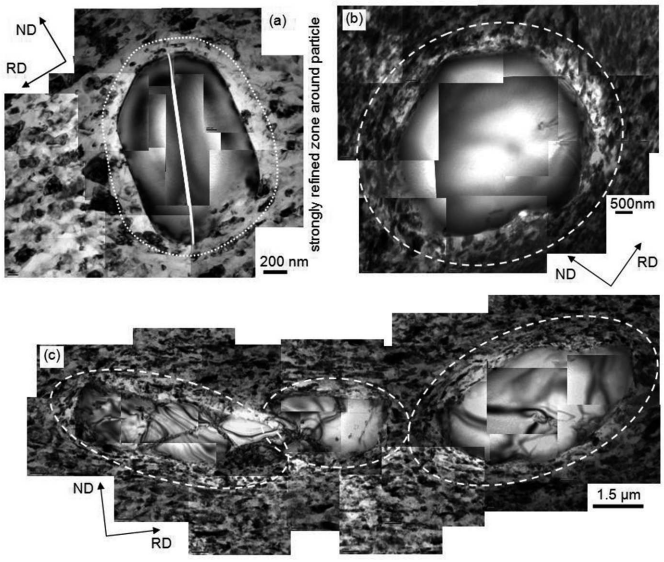

Fig. 6. Microstructures showing the formation of highly deformed zones near large SPPs. Samples deformed under 2 GPa after: (a) – 2 and (b) – 10 turns. (c) Clustering of highly deformed zones observed in the sample deformed under 3 GPa pressure after 4 turns. TEM bright field imaging. Dotted lines indicate strongly deformed zones around large particles

3.3. Recrystallization behaviour

3.3.1. Thermal analysis of the recrystallization process

Figure 7a shows the differential scanning calorimetry thermographs taken on a sample after 4 turns under the pressure of 3 GPa (curve – 1) together with a second run (curve – 2) on the as-quenched specimen. For the HPT-processed samples (1), only one low temperature exothermic maximum (~240°C) and one high temperature deep endothermic minimum (~364°C) are clearly visible. There are also some other weak peaks corresponding to different precipitation and dissolution processes. The as-quenched specimen (2) shows two endothermic peaks observed at the temperatures of 234°C and 376°C.

The DSC thermographs for the samples processed in 2, 6 and 10 turns under the pressure of 2 GPa are presented in Fig. 7b. The most important features observed in this thermographs are summarized below.

- The DSC curves coincide, thereby show the same recrystallization and precipitation/dissolution processes.
- All curves consist of one recrystallization exothermic peak at the temperature ranging between 240°C and 250°C and one endothermic high temperature minimum at the temperature ranging between 367°C and 372°C, correlated with the dissolution of the dispersoids.
- The peaks corresponding to the recrystallization process (marked by arrows) are shifted imperceptibly towards lower temperatures as the deformation increases.
- An additional exothermic peak at the temperature of ~300°C corresponding to the precipitation of the dispersoids is clearly visible only for the samples after 10 turns of the HPT-processing. The diameter of those small precipitates was a few tens of nanometers. They were preferentially located at the new grain/cell boundaries (Fig. 7c). In the recrystallization process they pinned the grain boundary migration and thus also new grain growth. This increases the thermal stability of the fine grained structures.
- The TEM/EDX point measurements reveal strong chemical composition changes between particular precipitates forming at the temperature of ~300°C. Most of the larger particles are characterized by increased contents of manganese, iron and silicon. The small precipitates, located in the new grain/cell boundaries, show increased contents of copper; this element is rarely observed in larger particles.

3.3.2. Bright field imaging in TEM for the study of recrystallization

The combination of thin foil heating and TEM-based orientation mapping makes it possible to correlate the microstructural changes with the evolution of orientations inside the small dislocation-free areas which appeared at the very early stages of recrystallization. In our TEM recrystallization experiments, it was frequently observed that the microstructure evolved rather uniformly due to the mechanism of continuous recrystallization. New grains, with clearly outlined recrystallization fronts, started to grow in the thicker areas of the thin foils at the later stages of annealing. The microstructure, after a short annealing, was coarser with respect to that observed in the deformed state. This was independent of the analyzed region of the sample, i.e. the axial or the peripheral regions.

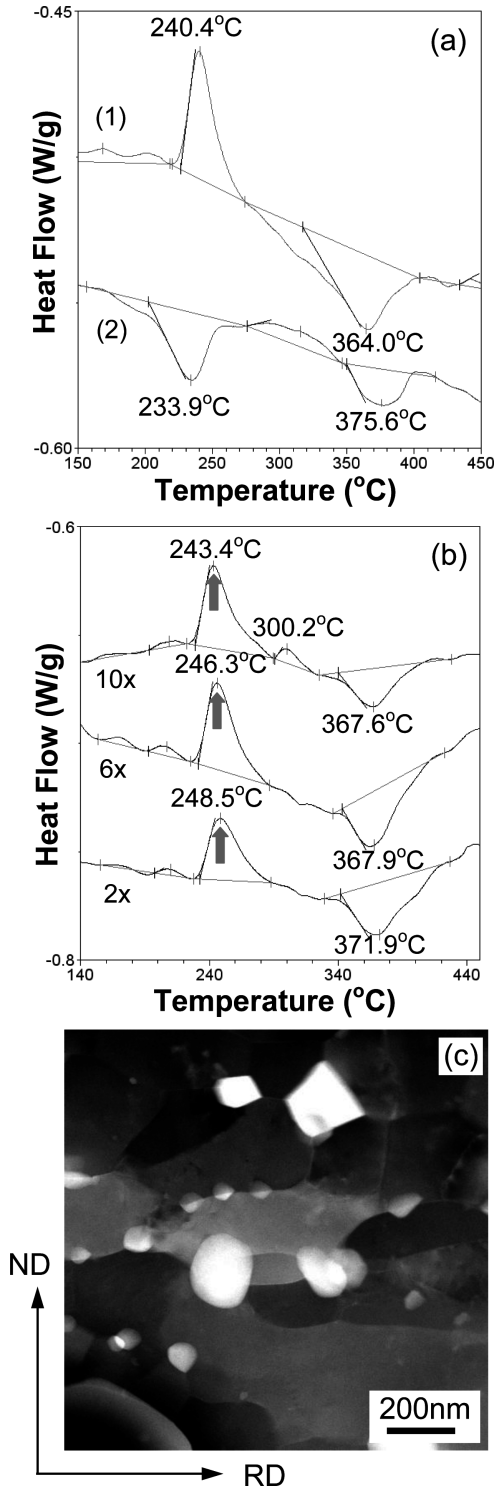

Fig. 7. (a) Temperature dependence of heat flow (DSC curves) for AA3104 alloy: (1) – the sample after 4 turns under 3 GPa pressure and (2) – the as-quenched specimen (second run). (b) DSC curves for the samples after 2, 6 and 10 turns of HPT under 2 GPa pressure. All samples were heated at a rate of 10 K min^{-1}. (c) HAADF-STEM microstructure showing precipitation of small dispersoids after heating at 300°C for 120 s

Figure 8 shows two cases of areas located close to (Fig. 8a) and far from (Fig. 8b) the large SPPs. It is visible that, after short annealing (at 300°C for 60 s), the structure was

composed of fine grains/cells of a similar size; the diameter ranged between 0.2 and 0.5 μm. This homogeneous structure was formed despite the highly deformed (and refined) zones around the large SPPs existing in the deformed state.

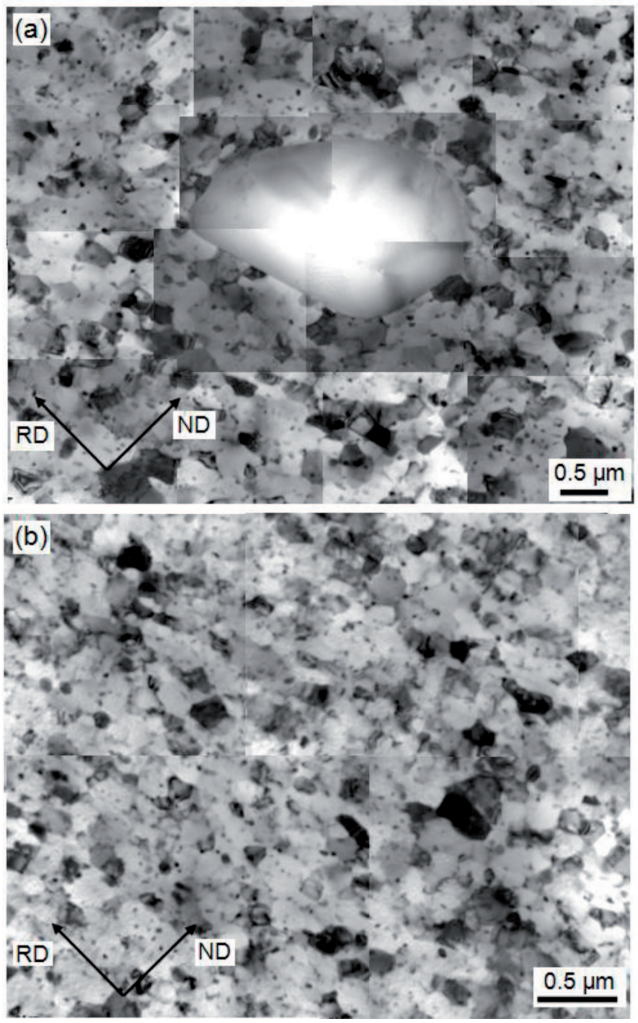

Fig. 8. TEM bright field images showing microstructures after recrystallization at 300°C for 60 s. Peripheral region (a) close to and (b) far from SPPs

3.3.3. TEM orientation mapping applied to the nano- scale study of recrystallization process

Attempts were made to investigate the texture of the deformed structures after the HPT-processing, but the Kikuchi patterns originating from them were too diffused for indexing, even after light heating at 100°C (similar effect was observed in the previous study on the same alloy but processed by ECAP [28]). In consequence, the orientation maps were not suitable for drawing any important conclusions on the orientation evolution during deformation, and these changes are not discussed here. The possibility of local orientation measurements was significantly improved after the recrystallization at ~300°C. The orientation maps were measured on thin foils cut out from selected areas of the sample along the sections perpendicular to the compression plane. All the orientation maps were presented as a 'function' of the IPF colour code. The bold black lines indicate the high-angle grain boundaries, i.e. >15° (HAGBS) whereas the thin black lines – the low-angle boundaries, i.e. <15° (LAGB) on all the orientation maps. (As regards the *in-situ* heating experiment in TEM, it should be noted that the recrystallization dynamics depend on the specimen thickness, as discussed in, e.g. [28]).

Figures 9a and b show the orientation map measured with the step size of 20 nm in the sample processed in one turn under the pressure of 2 GPa and the corresponding {111} pole figure. The thin foils were cut out from the central area of the sample along the ND-RD section and annealed at 300°C for 30 s. The orientation imaging system very well revealed the elongated character of grains subdivided by the network of LAGB. The {111} pole figure corresponding to the orientation map clearly shows that the <111> crystallographic directions are parallel to ND.

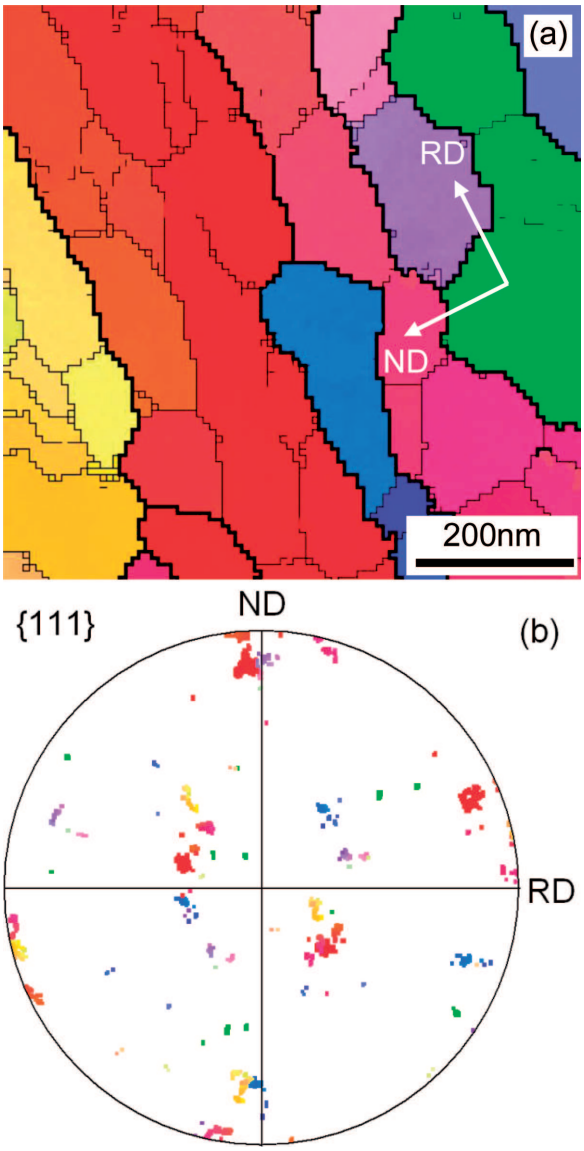

Fig. 9. (a) TEM orientation map and (b) corresponding {111}pole figure measured in the axial area of the sample. The sample processed in one turn under 2 GPa pressure and then annealed at 300°C for 30 s. TEM local orientation measurements with step size of 20 nm in ND-RD section. IPF colour code was applied

Similar microstructures were observed in the tangential section (ND-TD) of the peripheral region of the sample

processed in one turn. As an example, Figure 10 presents two orientation maps and corresponding the {111} pole figures measured in the areas far from (Fig. 10a and c) and close to (Fig. 10b and d) the large SPPs at a radius of about 11 mm. The maps were made with the step size of 10 nm on thin foil annealed for 30 s at 300°C; it can be seen that the microstructures are far from equiaxed. The recovered[2)], elongated areas, separated by HAGB's, are well-revealed by the orientation imaging system. Since the recovered and deformed areas are described by the same orientation groups [18, 19], the tracking of the orientation evolution during annealing was possible. The orientations of the layers separated by HAGB's were nearly twin related (in fact, complementarily oriented), as presented in Figs. 10c and d. The disorientation line scan along the elongated cells approached 10-12° (Fig. 10e), whereas the line scan across the cells showed larger disorientations, which very

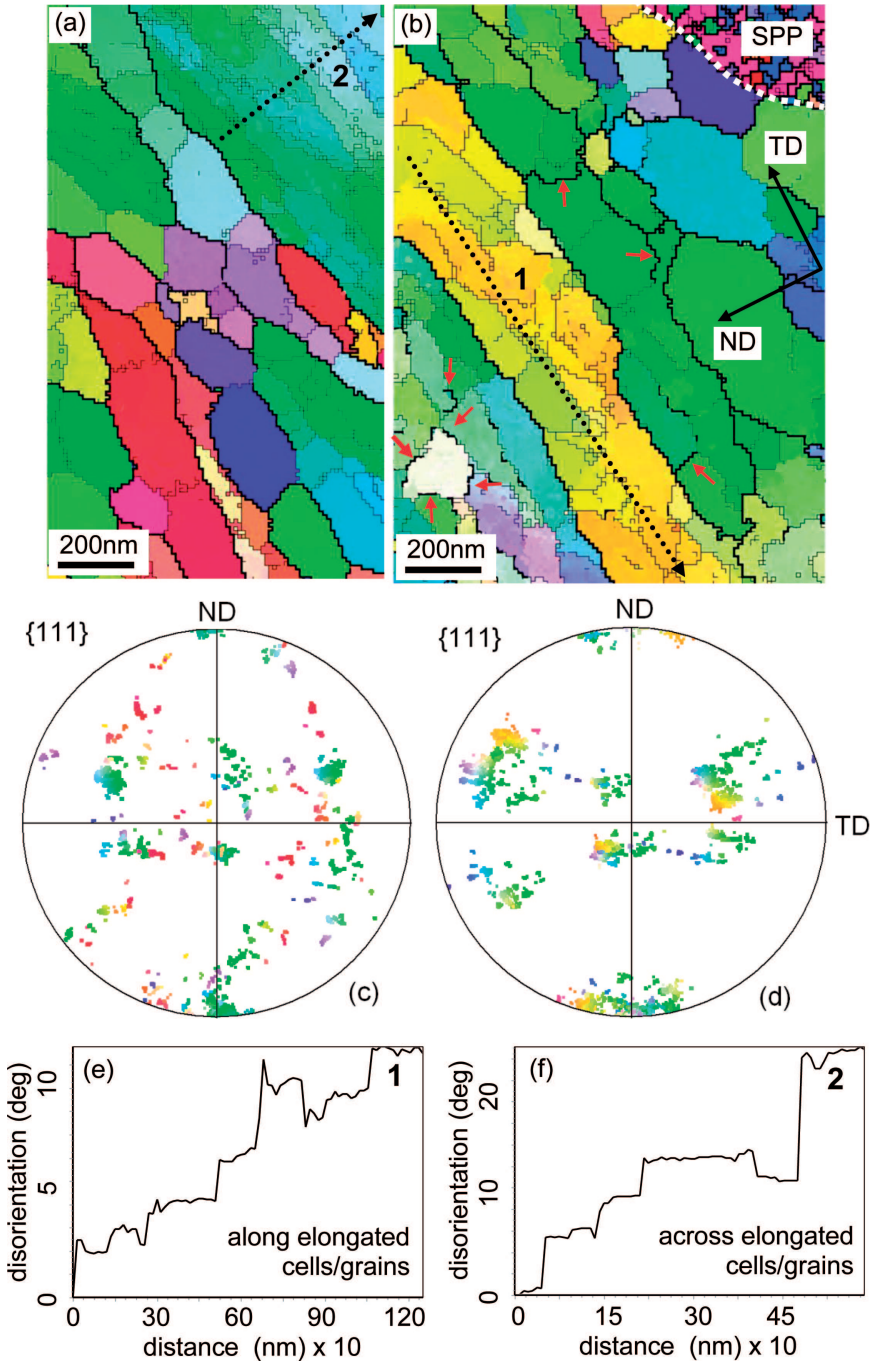

Fig. 10. Microstructures and textures observed in the central region of the sample processed in one turn under 2 GPa pressure and then annealed at 300°C for 30 s. Orientation maps and corresponding {111} pole figures made in (a) and (c) far from large SPPs and (b) and (d) close to large SPPs. (e) and (f) disorientation line scans showing disorientations (with respect to the first measured point) measured across and along elongated cells observed in (a) and (b), respectively. TEM local orientation measurements with 20 nm step size in ND-TD section. IPF colour code was applied

[2)] It is assumed here that these areas were only recovered since they were subdivided by an additional network of low angle grain boundaries.

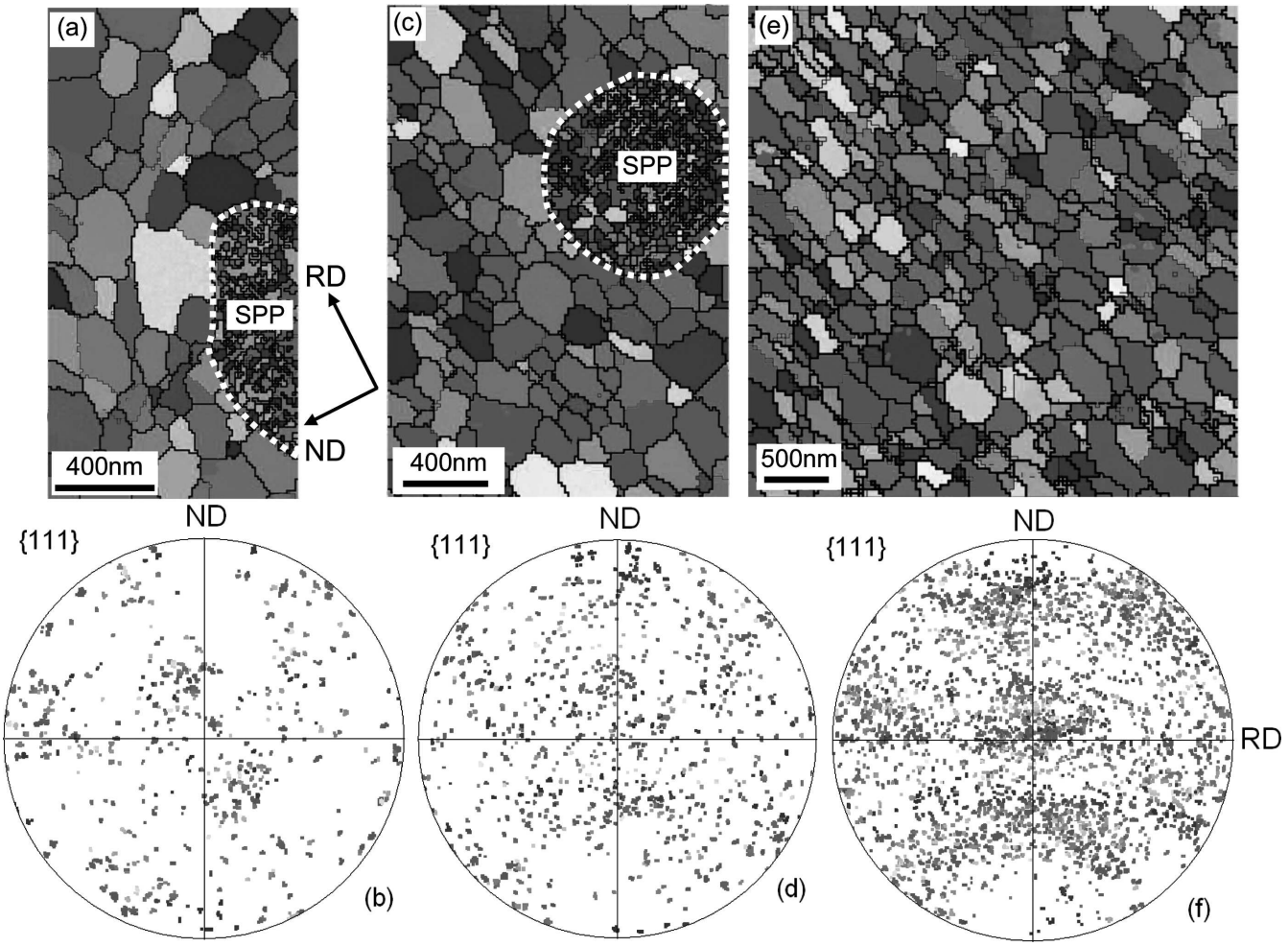

Fig. 11. Microstructure and texture observed in the central region of the sample processed in 10 turns under 2 GPa pressure and then annealed at 300°C for 60 s. Orientation maps in areas: (a) close to large plate shaped SPPs, (b) close to nearly globular large SPPs and (c) far from large SPPs and (d)-(f) corresponding {111}pole figures. TEM local orientation measurements with 20 nm and step size in ND-RD section. IPF colour code was applied

often reached 20-25° (Fig. 10f). In some places, the equiaxed areas surrounded by HAGB's were also observed (red arrows in Fig. 10b). They can be assigned to the new grains that start to grow after heating. The orientations typically observed in the areas of the deformed/recovered state (containing an additional network of LAGB's) were grouped near the components of the <111> axial texture, as visible in Figs. 10c and d. For the samples deformed in one turn, most of the recrystallized grains grow from the pre-existing cells. At the first stage of the new recrystallized grain formation, some parts of the low angle boundaries accumulate dislocations, and the nuclei become increasingly disoriented with respect to their neighbours (the red arrows in Fig. 10b indicate the fragments of the grain boundaries with increased disorientation). This increases the energy and mobility of grain boundaries [32, 33].

Figure 11 shows the orientation maps made with the step size of 20 nm measured in three characteristic places, i.e. in the area near the tips of the plate shaped SPPs, nearly globular ones and in the area far from the large SPPs. The thin foils were cut-off along the ND-RD section at the sample periphery from the sample deformed in ten turns under the pressure of 2 GPa and then annealed at 300°C for 60 s. In the area close to the tips of the large SPPs, only the recrystallized and nearly equiaxed grains, with the diameter of 100-200 nm, were observed (Fig. 11a). The 150×80 pixel orientation map shows the arrangements of the new grains which still imitate the structure 'directionality', typically observed in the deformed state.

The {111} pole figure presented in the ND-RD co-ordinate system (Fig. 11b) shows that the directions of <110>-type are mostly perpendicular to the thin foil plane. Moreover, in most cases an increased density of the orientations with the <100> direction nearly parallel to ND was observed.

The area close to the globular SPPs was characterized by a 100×150 pixel map, Fig. 11c. In that case, the structure of the equiaxed grains of a similar size completely lost the tendency to 'flow around' the large SPPs. The diameters of the grains ranged between 100 nm and 300 nm, whereas the grain orientations showed a clear tendency to increase the densities of the <100> directions close to ND, as observed on the {111} pole figure (Fig. 11d). Figure 11e is a 150 x 150 pixel map which shows the structure of the fully recrystallized grains observed in the areas placed far from the large SPPs. The shape of the grains is slightly elongated along RD and the new grain orientations lost the positions typical for the

deformed state. Although the textures are scattered, some preferences in the selection of the new grain orientations are observed. Those preferences are associated with the coincidence of the <100> and <110> crystallographic directions with ND (in those cases, the <110> and <111> crystallographic directions were parallel to the thin foil normals).

The distribution of the disorientation angles and disorientation axes strongly depends on the recrystallization progress. In the partly recrystallized areas, the distribution of the disorientation angles between particular pixels reveals a relatively large fraction of low (<15°) LAGB and an increased frequency of the boundaries with the disorientation angles close to 45-50° (Fig. 12a), as typically observed in the deformed state. A large fraction of the boundaries with the disorientation angles close to 40° was revealed in the more advanced stages of the recrystallization (Fig. 12b). Both cases reflect the near-random distribution of the disorientation axes in the relation between particular pixels of the orientation maps (for angles larger than 1.5°). However, the disorientation relations across the recrystallization front were not random and the disorientation axes were grouped near specific crystallographic directions (see section 4.2).

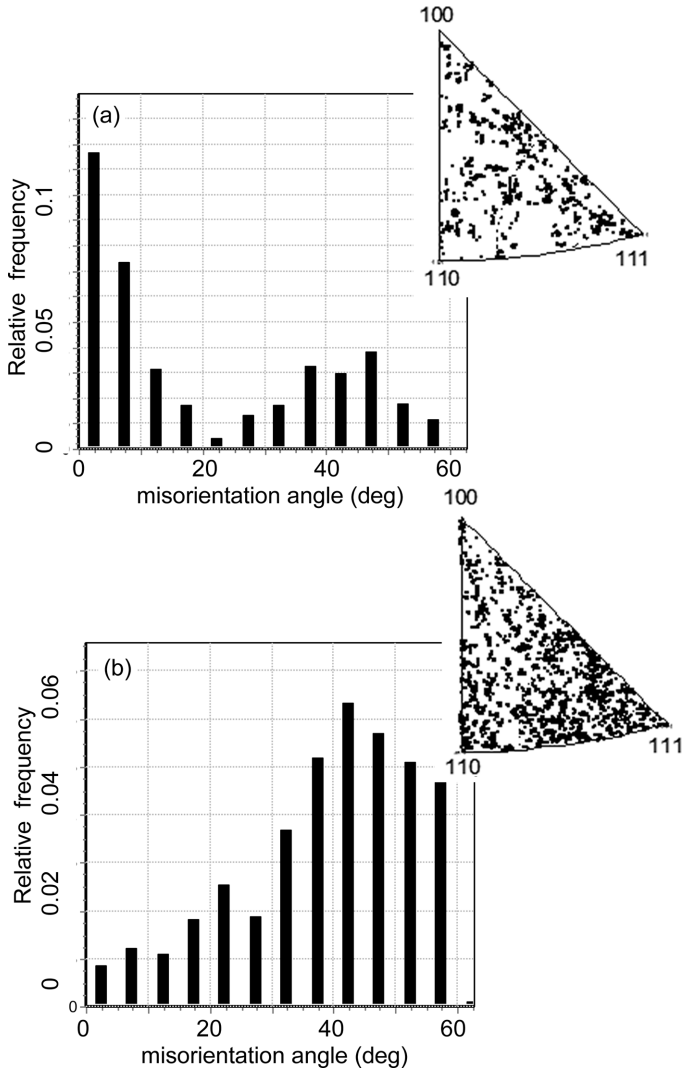

Fig. 12. The distributions of the disorientation angles and axes observed in (a) only recovered and (b) fully recrystallized areas, corresponding to orientation maps of Figs. 10b and 11a, respectively

3.3.4. Microstructure evolution analysed by SEM/EBSD

All recrystallized bulk samples exhibited microstructures with a clear separation between the deformed/recovered areas and the recrystallized grains. The orientation maps presented in Fig. 13 show the microstructures observed in the ND-RD section of the samples deformed in 10 turns under the pressure of 3 GPa and then annealed. After the recrystallization at 300°C for 60 s (Fig. 13a), the structure was composed of areas where continuous and discontinuous recrystallization occurred. Most of the new recrystallized grains (in the form of separate grains or grain chains), with well-defined boundary, attain dimensions ranging between 2 μm and 3 μm, whereas the dimensions of the strongly recovered cells of the deformed state were still significantly below 300-500 nm. After the annealing at 300°C for 300 s, only new recrystallized grains were observed. The orientation map presented in Fig. 13b well documents the homogeneous distribution of the very small recrystallized grains of the average diameter close to 2 μm (Fig. 13c) with the near-random orientation distribution (Fig. 13d).

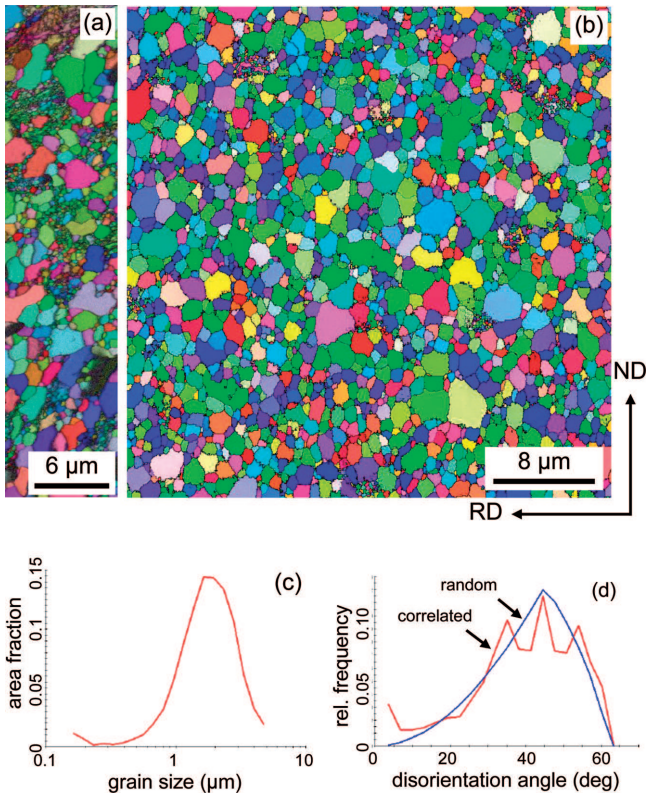

Fig. 13. Early stages of recrystallization observed in areas near the sample periphery. Sample deformed in 10 turns under pressure of 3 GPa and then recrystallized at 300°C for: 60 s (a) and 300 s (b). The distribution of grain sizes (c) and disorientation angles (d). SEM/EBSD local orientation measurements with step size of 100 nm. IPF colour code is applied

4. Discussion

4.1. Microstructure and texture of the deformed state

The present paper demonstrates excellent grain refinement of the AA3104 alloy after the HPT processing and

clearly reveals the dependence of the microstructure on the amount of deformation and the applied pressure. The large flat grains, typically observed after hot rolling, just after two first turns, were 'transformed' into more or less equiaxed small grains. The gradual evolution towards a perfectly homogeneous fine-grained structure occurs at the deformations higher than 5-6 turns. This is consistent with the earlier experimental data reported, e.g. for pure aluminium and aluminium alloys [4, 8, 34-37], high purity copper and copper alloys [13-17, 38, 39], nickel [40, 41], steel [42, 43], etc.

In the present work the answer to the question – *how the orientation of initially formed grains has been affected (if at all) by the orientation identified inside neighbouring deformed (or recovered) areas* is based on the description of the relation between the texture images of the deformed/recovered and the recrystallized 'phase'. The texture 'image' of the deformed/recovered areas was composed of two well-marked texture fibers of the {111} and <011>-type, i.e. two fibres dominating torsion type texture. In the classical description of the torsion texture development in fcc metals, two texture fibers, namely {111}<*uvw*> and {*hkl*}<110>, play an important role [44, 45] (the notation of {*hkl*}<*uvw*> refers to the set of planes and directions parallel to the shear plane (compression plane in HPT) and the shear (here tangential) direction, respectively). The strong {111}-type fibre (with increased densities close to the {111}<110> orientation) developing during the early stages of the HPT-deformation was also observed earlier, in pure Al [23] and electrodeposited Ni [22]. However, during further processing, the intense grain growth in the volumes near the sample periphery (due to spontaneous recrystallization) leads to the creation of new texture components that do not exhibit positions typically observed in the deformed state.

4.2. Disorientation relation at early stages of recrystallization

The orientations of the dislocation free areas surrounded by the high-angle grain boundaries are different from the orientations of the deformed state, as presented many times in the past, e.g. [18, 19]. The present work shows that the texture components with the <111> directions parallel to ND were characteristic for the deformed/recovered areas. With the progress of the recrystallization, the increase of the <100> fibre[3)] and the disappearance of the texture components connected with the deformed/recovered state were observed. The rotation axes of the disorientations across the recrystallization front are scattered, as presented in Fig. 12, but some preferences are observed. The nearly equiaxed grains have orientations which (in most of the analyzed cases) can result from the rotations around the axes close to <122> and <012> with respect to the texture components characteristic for the deformed/recovered state. The disorientation axes close to <011>, <112> and the 'classical' <111> positions were also (but rarely) detected. The analysis of the TEM and SEM orientation maps indicates that the <111>-type rotation occurs more often at the later stages of the recrystallization, at which the fraction of the boundaries between the recrystallized grains grows. For a particular case of a fully recrystallized structure (as observed in Fig. 11) with the near-random disorientation distribution, the distribution of the disorientation angles has the maximum near the 40° angle, as predicted theoretically by Mackenzie [46].

4.3. Crystallographic aspect of new grains occurring near and far from large SPPs

Orientation mapping is a suitable method which could be used to resolve the question: *is the structure and the texture similar in the areas close to and far from the large SPPs after annealing*? The bright field image of Fig. 8 and the orientation maps of Figs. 7, 8 and 11 clearly show that the microstructures after annealing were characterized by a similar grain size and the same high level structural homogeneity. It happens regardless of the fact that the structural inhomogeneity appears just after the deformation.

A direct comparison of the orientations of the grains placed close to and far from the large SPPs was performed on the basis of many TEM orientation maps and the result of this analysis is presented in Fig. 14. It is evident that the textures detected in both areas were generally similar; only a slightly larger scattering of the orientation of the new grains placed close to the large SPPs was observed. The recrystallization textures measured at the 'end stage' of the primary recrystallization[4)] (as presented in Fig. 7b) were qualitatively similar to the textures observed in the electro-deposited nano-crystalline Ni and the coarse grained Ni subjected to HPT [21, 22]. Those similarities results from the dominance of the duplex <111> and <100> fiber texture (i.e. the <111> and <100> crystallographic directions were parallel to ND). Yang et al. [21] stated that the formation of the submicron-sized structure and the 'final shape' of the deformation texture are the result of '*...a competition between coarsening by deformation-induced high angle grain boundaries migration and fragmentation by dislocation induced shear deformation*'. Since the authors observed structure coarsening due to the movement of the boundaries, an explanation of the texture formation based only on the deformation behaviour seems to be disputable. In our opinion, the events observed in the HPT-processed Ni [21, 22] resulted from 'the room temperature recrystallization'. The new grain nucleation and the intense grain boundary migration occur due to the high stored energy of deformation and the relatively high stacking fault energy of Ni. The increased density of the components forming the {111}-type fiber is typical for the shear texture formation, but the {100}<*uvw*> texture components are related to the recrystallized grains. This 'room temperature annealing' was also observed earlier in pure copper plane strain compressed at 77 K and Cu-2%Al alloy single crystals [47] or silver ECAP-ed at room temperature [48]. It is worth to mention, that the data can be employed in development of numerical models like digital material representation, which mostly relay on crystal plasticity material model description [49, 50].

---

3) the new grain orientations evolve in such a way that the <100>crystallographic direction coincides with ND (Fig. 11)

4) when the areas of the deformed state are completely 'consumed'

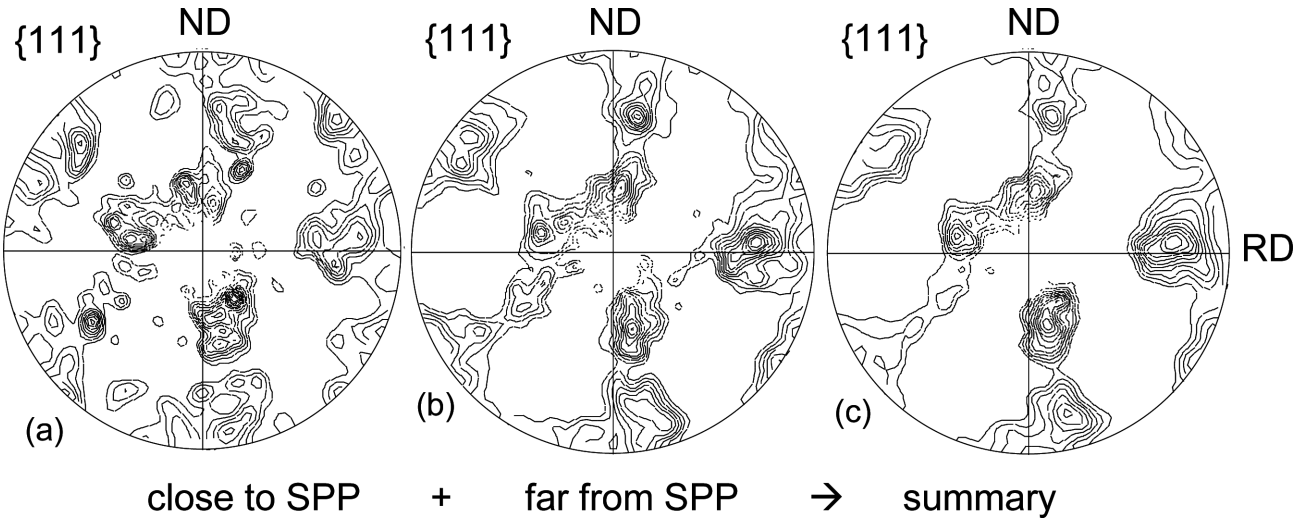

Fig. 14. The {111}pole figures showing textures of grains appearing in areas (a) close to and (b) far from large SPPs. (c) Summarized texture of both areas. TEM local orientation measurements

In HPT-processed materials, the final shape and size of the grains seem to be a competition between the fragmentation by the shear deformation and the coarsening by the grain boundary migration. The grain boundary migration seems to be inherently linked to the recrystallization process [18, 19]. The strains needed to initiate boundary migration and significant grains coarsening are relatively large. It was observed here that in the samples deformed in over six turns the room temperature recrystallization often occurred in the peripheral areas of the sample whereas the axial areas still remained in as-deformed[5)] state. In the peripheral areas, the grains attain their large sizes (in comparing to the central areas) and this process coincides with the decrease of the microhardness and the strong textural changes, as observed earlier in, e.g. [2]. The intense cooling of the die during the processing strongly limited the dynamic recrystallization during the HPT-processing. This leads to higher stored energy of deformation which is later violently released when the processing is completed. Therefore, in the periphery sample volumes (the volumes of very high stored energy of deformation) recrystallization is stronger than in regions closer to the sample axis. The recrystallization is the likely reason of the microhardness decrease in the sample periphery of the HPT-processed (up to high deformations) samples, as observed in pure aluminium, e.g. [2, 51] (in highly deformed pure aluminium, the discs exhibited a smaller grain size in the central region of the disc than that observed in the outer regions).

5. Summary

This paper describes the structure refinement by HPT processing and the crystallographic aspect of microstructure coarsening at the early stages of recrystallization. Individual grain orientations in slightly annealed structures of the AA3104 aluminium alloy containing a complex structure of second phase particles were measured with the use of TEM-based orientation mapping in combination with recrystallization carried out in TEM. The main results are summarized below:

- The microstructure of the AA3104 alloy shows a gradual evolution to a homogeneous structure with the increase of the strain (number of turns) and/or the applied pressure. The size of the grain/cell decreases with the increasing strain and the applied pressure. After six turns, a perfectly uniform structure of fine grains is observed in the sample (except sample edge), and the size of the microstructural elements reaches the steady-state value. The crystal lattice of the small grains rotates in such a way that the <111> crystallographic direction is parallel to the compression axis.
- The shear deformation effects are particularly strong in the areas of the matrix close to the plate shaped coarse particles.
- Grains of a similar size were observed after annealing regardless of the fact that highly deformed zones around the large SPPs appeared after the deformation. The precipitation of dispersoids occurring at the temperature close to 300°C strongly hinders the grain growth during the primary recrystallization.
- The orientations of the new grains were different from those in adjoining deformed/recovered neighbourhood. The new grains show the tendency to the coincidence of the <100> crystallographic direction with the ND.
- The difference between the new grain textures measured in areas close to and far from the SPPs at the 'end' of the primary recrystallization stage was small; only negligibly larger scattering of orientations of the new grains placed close to the SPPs was observed.
- This work confirms that, despite the difficult sample preparation, TEM is a useful tool for the texture analysis in the nano-scale. Because of the diffused diffraction patterns, TEM-based orientation measurements could not be directly applied to the highly deformed areas of the HPT-processed samples. The situation was significantly improved after the annealing of the foils. In that case the

[5)] This indicates that the peripheral areas undergo a more intense plastic deformation than the axial ones

quality of the orientation maps was on the acceptable level, even in the areas close to the large SPPs.

Acknowledgements

The financial support from National Centre of Science (project no: 2014/13/B/ST8/04291) is gratefully acknowledged. The HPT tests were performed by using tensile testing machine Zwick 1200 – purchase in the range of the project co-financed by European Union (project no: POIG.02.01.00-12-175/09). The authors are grateful to Dr M. Bijak for the help in the HPT sample processing and Dr M. Miszczyk – for the thin foil preparation.

REFERENCES

[1] R.Z. Valiev, R.K. Islamgaliev, I.V. Aleksandrov, Bulk nanostructured materials from severe plastic deformation, Progr. Mater. Sci. **45**(2), 103-189 (2000).

[2] A.P. Zhilyaev, T.G. Langdon, Using high-pressure torsion for metal processing: Fundamentals and applications, Prog. Mat. Sci. **53**, 893-979 (2008).

[3] I. Sabirov, M.Yu. Murashkin, R.Z. Valiev, Nanostructured aluminium alloys produced by sever plastic defromation: New horizons in development, Mat. Sci. Engn. A **560**, 1-24 (2013).

[4] M.J. Starink, X. Cheng, S. Yang, Hardening of pure metals by high-pressure torsion: A physically based model employing volume-average defect evolutions, Acta Mater. **61**, 183-191 (2013).

[5] J. Zhang, N. Gao, M.J. Starink, Micostructure development and hardening during high pressure torsion of commercially pure aluminium: strain reversal experiments and a dislocation based model, Mat. Sci. Engn. A **528**, 2581-2591 (2011).

[6] J. Zhang, M.J. Starink, N. Gao, W. Zhou, Effect of Mg addition on strengthening of aluminium alloys subjected to different strain paths in high pressure torsion, Mat. Sci. Engn. A **528**, 2093-2099 (2011).

[7] A. Loucif, R.B. Figueiredo, T. Baudin, F. Brisset, R. Chemam, T.G. Langdon, Ultrafine grains and the Hall-Petch relationshop in an Al-Mg-Si alloy processed by high-pressure torsion, Mat. Sci. Engn. A **532**, 139-145 (2012).

[8] A. Loucif, R.B. Figueiredo, T. Baudin, F. Brisset, T.G. Langdon, Microstructural evolution in an Al-6061 alloy processed by high-pressure torsion, Mat. Sci. Engn. A **527**, 4864-4869 (2010).

[9] E.C. Moreno-Valle, I. Sabirov, M.T. Perez-Prado, M.Y. Murashkin, E.V. Bobruk, R.Z. Valiev, Effect of the grain refinement via sever plastic deformation on strength properties and deformation behaviour of an Al6061 alloy at room and cryogenic temperatures, Materials Letters **65**, 2917-2919 (2011).

[10] A. Loucif, R.B. Figueiredo, T. Baudin, F. Brisset, R. Chemam, T.G. Langdon, Effect of ageing on microstructural development in an Al-Mg-Si alloy processed by high-pressure torsion, J. Mater. Sci. **47**, 7815-7820 (2012).

[11] S. Sabbaghianrad, M. Kawasaki, T.G. Langdon, Microstructural evolution and the mechanical properties of aluminum alloy processed by high-pressure torsion, J. Mater. Sci. **47**, 7789-7795 (2012).

[12] M. Eddahbi, A. Borrego, M.A. Monge, G. González-Doncel, Microstructure gradient after hot torsion deformation of powder metallurgical 6061 alloy, Mat. Sci. Engn. A **555**, 154-164 (2012).

[13] N. Lugo, N. Llorca, J.M. Cabrera, Z. Horita, Microstructures and mechanical properties of pure copper deformed severely by equal-channel angular pressing and high pressure torsion, Mat. Sci. Engn. A **477**, 366-371 (2008).

[14] X.H. An, S.D. Wu, Z.F. Zhang, R.B. Figueiredo, N. Gao, T.G. Langdon, Evolution of microstructural homogeneity in copper processed by high-pressure torsion, Scripta Mater. **63**, 560-563 (2010).

[15] T. Hebesberger, H.P. Stüwe, A. Vorhauer, F. Wetscher, R. Pippan, Structure of Cu deformed by high pressure torsion, Acta Mater. **53**, 393-402 (2005).

[16] Y.Z. Tian, J.J. Li, P. Zhang, S.D. Wu, Z.F. Zhang, M. Kawasaki, T.G. Langdon, Microstructures, strengthening mechanisms and fracture behaviour of Cu-Ag alloys processed by high-pressure torsion, Acta Mater. **60**, 269-281 (2012).

[17] J. Wongsa-Ngam, M. Kawasaki, T.G. Langdon, Achieving in homogeneity in a Cu-Zr alloy processed by high-pressure torsion, J. Mater. Sci. **47**, 7782-7788 (2012).

[18] F.J. Humphreys, M. Hatherly, Recrystallization and Related Annealing Phenomena, 2^{nd} edition, Elsevier Ltd, Oxford, UK, 2003.

[19] R.D. Doherty, D.A. Hughes, F.J. Humphreys, J.J. Jonas, D. Juul Jansen, M.E. Kassner, W.E. King, T.R. McNeally, H.J. McQueen, A.D. Rollett, Current issues in recrystallization: A review, Mat. Sci. Engn. A **238**, 219-274 (1997).

[20] O. Engler, X.W. Kong, K. Lücke, Recrystallization textures of particle-containing Al-Cu and Al-Mn single crystals, Acta Mater. **49**, 1701-1715 (2001).

[21] B. Yang, H. Vehoff, A. Hohenwarter, M. Hafok, R. Pippan, Strain effects on the coarsening and softening of electrodeposited nanocrystalline Ni subjected to high pressure torssion, Scripta Mater. **58**, 790-793 (2008).

[22] X.Z. Liao, A.R. Klimametov, R.Z. Valiev, H. Gao, X. Li, A.K. Murherjee, J.F. Bingert, Y.T. Zhu, High-pressure torsion-induced grain growth in electrodeposited nanocrystalline Ni, Appl. Phys. Lett. **88**, 021909 (2006).

[23] D. Orlov, P.P. Bhattacharje, Y. Todaka, M. Umemoto, N. Tsuji, Texture evolution in pure aluminium subjected to monotonous and reversal straining in high-pressure torsion, Scripta Mater. **60**, 893-896 (2009).

[24] Z. Yao, G. Huang, A. Godfrey, W. Liu, Dislocation boundary structure from low to medium strain of cold rolling AA3104 aluminum alloy, Metall. Mater. Trans. A **40A**, 1487-1497 (2009).

[25] Q. Liu, Z. Yao, A. Godfrey, W. Liu, Effect of particles on microstructural evolution during cold rolling of the aluminium alloy AA3104, Journal of Alloys and Compounds **482**, 264-271 (2009).

[26] W.C. Liu, P.P. Zhai, Characterization of microstructures near grain boundary in hot deformed AA3104 aluminium alloy, Mater. Character **62**, 81-89 (2011).

[27] H. Paul, T. Baudin, F. Brisset, Effect of strain path and second phase particles on microstructure and texture evolution of AA3104 aluminum alloy processed by ECAP, Arch. Metall. Mater. **56**, 245-261 (2011).

[28] H. Paul, A. Morawiec, T. Baudin, Early stages of recrystallization in ECAP-deformed AA3104 alloy investigated using SEM and TEM orientation mappings, Metall. Mater. Trans. A **43A**, 4777-4793 (2012).

[29] S. Bhaumik, X. Molodova, G. Gottstein, Effect of stress and the annealing behaviour of severely plastically deformed aluminum alloy 3103, Mat. Sci. Engn. A **527**, 5826-5830 (2010).

[30] A. Etienne, B. Radiguet, C. Genevois, J-M. Le Breton, R. Valiev, P. Pareige, Thermal stability of ultrafine-grained austenitic stainless steels, Mat. Sci. Engn. A **527**, 5805-5810 (2010).

[31] Y.Z. Tian, S.D. Wu, Z.F. Zhang, R.B. Figueiredo, N. Gao, T.G. Langdon, Strain hardening behavior of a two-phase Cu–Ag

alloy processed by high-pressure torsion, Acta Mater. **59**, 2783-2796 (2011).

[32] P.A. Beck, Notes on the theory of annealing textures, J. Appl. Phys. **20**, 633-634 (1949).

[33] R.W. Cahn, A new theory of recrystallization nuclei, Proc. Phys. Soc. A **63**, 323-336 (1950).

[34] C. Xu, Z. Horita, T.G. Langdon, The evolution of homogeneity in processing by high-pressure torsion, Acta Mater. **55**, 203-212 (2007).

[35] E.C. Moreno-Valle, I. Sabirov, M.T. Perez-Prado, M.Y. Murashkin, E.V. Bobruk, R.Z. Valiev, Effect of the grain refinement via severe plastic deformation on strength properties and deformation behavior of an Al6061 alloy at room and cryogenic temperatures, Materials Letters **65**, 2917-2919 (2011).

[36] B.B. Straumal, B. Baretzky, A.A. Mazilkin, F. Phillipp, O.A. Kotgenkova, M.N. Volkov, R.Z. Valiev, Formation of nanograined structure and decomposition of supersaturated solid solution during high pressure torssion of Al-Zn and Al-Mg alloys, Acta Mater. **52**, 4469-4478 (2004).

[37] B. Straumal, R. Valiev, O. Kotgenkova, P. Zięba, T. Czeppe, O. Bielańska, M. Faryna, Thermal evolution and grain boundary phase transformations in severely deformed nanograined Al-Zn alloys, Acta Mater. **56**, 6123-6131 (2008).

[38] K. Edalati, T. Fujioka, Z. Horita, Microstructure and mechanical properties of pure Cu processed by high-pressure torsion, Mater. Sci. Engn. A **497**, 168-173 (2008).

[39] N. Lugo, N. Llorca, J.M. Cabrera, Z. Horita, Microstructures and mechanical properties of pure copper deformed severely by equal-channel angular pressing and high pressure torsion, Mat. Sci. Engn. A **477**, 366-371 (2008).

[40] A.P. Zhilyaev, G.V. Nurislamova, B.K. Kim, M.D. Baró, J.A. Szpunar, T.G. Langdon, Experimental parameters influencing grain refinement and microstructural evolution during high-pressure torsion, Acta Mater. **51**, 753-765 (2003).

[41] F. Dalla Torre, P. Spätig, R. Schäublin, M. Victoria, Deformation behaviour and microstructure of nanocrystalline electrodeposited and high pressure torsioned nickel, Acta Mater. **53**, 2337-2349 (2005).

[42] A. Vorhauer, R. Pippan, On the homogeneity of deformation by high pressure torsion, Scripta Mater. **51**, 921-925 (2004).

[43] Y. Cao, Y.B. Wang, R.B. Figueiredo, L. Chang, X.Z. Liao, M. Kawasaki, W.L. Zheng, S.P. Ringer, T.G. Langdon, Y.T. Zhu, Three-dimensional shear-strain patterns induced by high-pressure torsion and their impact on hardness evolution, Acta Mater. **59**, 3903-3914 (2011).

[44] F. Montheillet, M. Cohen, J.J. Jonas, Axial stresses and texture development during the torsion testing of Al, Cu and α-Fe, Acta Metall. **32**, 2077-2089 (1984).

[45] L.S. Tóth, K.W Neale, J.J. Jonas, Stress Response and Persistence Characteristics of the Ideal Orientations of Shear Textures, Acta Metall. **37**, 2197-2210 (1989).

[46] J.K. Mackenzie, The distribution of rotation axes in a random aggregate of cubic crystals, Acta Metall. **12**, 223-225 (1964).

[47] H. Paul, J.H. Driver, C. Maurice, Z. Jasieński, Crystallographic aspects of the early stages of recrystallization in brass type shear bands, Acta Mater. **50**, 4339-4355 (2002).

[48] J. Gubicza, N.Q. Chinh, J. Lábar, Z. Hegedüs, T.G. Langdon, Principles of self-annealing in silver processed by equal-channel angular pressing: The significance of a very low stacking fault energy, Mat. Sci. Engn. A **527**, 752-760 (2010).

[49] W. Wajda, Ł. Madej, H. Paul, R. Gołąb, M. Miszczyk, Validation of texture evolution model for polycrystalline aluminium on the basis of 3D digital microstructures, Steel Research International, Special Edition 1111-1114 (2012).

[50] W. Wajda, Ł. Madej, H. Paul, Application of Crystal Plasticity Model for Simulation of Polycrystalline Aluminium Sample Behaviour During Plain Strain Compression Test, Arch. Metall. Mater. **58**, 493-496 (2013).

[51] A.P. Zhilyaev, K. Oh-Ishi, T.G. Langdon, T.R. McNelley, Microstructural evolution in commercial purity aluminum during high-pressure torsion, Mat. Sci. Engn. A **410-411**, 277-281 (2005).

Received: 20 March 2014.